Magnetoplasma absorption of intense electromagnetic waves: Numerical results

A. L. Peratt*
Lawrence Livermore Laboratory, University of California, Livermore, California 94550
(Received 28 June 1978)

Numerical methods are used to investigate absorption of either intense or weak electromagnetic waves obliquely incident on a nonuniform plasma with and without the presence of a dc magnetic field. The numerical formulation includes the full set of Maxwell's equations and three moments of the Boltzmann equation with a ponderomotive-force description. The investigation includes a study of the reflection and absorption of the incident wave as a function of angle of incidence as well as the complex electric and magnetic fields, electron-flow, dc magnetic field generation, and kinetic energy gained by resonant electrons within the plasma. Selected field snapshots are directly compared to particle-simulation predictions where a thousandfold reduction in computation time allows a detailed investigation of the wave-plasma interaction for laser wavelengths.

INTRODUCTION

The conversion, resonance, and absorption of electromagnetic waves in an inhomogeneous plasma is fundamental to understanding energy transfer in fusion reactor models for either magnetic-confinement fusion using GHz high-power sources or for fusion by laser, where an intense light wave is obliquely incident on a solid inertial confinement pellet.[1,2] The mode conversion process is important to the high-frequency electromagnetic–wave–plasma interaction because, while an incident electromagnetic wave cannot resonantly transfer energy to the plasma particles, the plasma wave excited by the electromagnetic wave can. Also, exciting plasma waves is generally an efficiently means of heating. This same effect is also of concern to inertial-confinement configurations.

In the study of intense waves interacting with plasma, researchers have almost exclusively used plasma-simulation codes, which model the collective interactions of a large number of discrete plasma particles with themselves and with external electromagnetic forces.[3] Often, the size of the plasma that can be simulated in detail is limited by the available computer time and memory. For example, studying cyclotron harmonic effects may require many particles and hence excessive computer time.[4] Furthermore, in the numerical data from a simulation, the individual physical mechanisms at work are often not clearly distinguished.

In this paper I derive formulas, based on a kinetic theory approach, that describe quantitatively the strength of the excited plasma waves and the role they play in the resonant absorption of electromagnetic waves in a nonuniform plasma, with and without the presence of a dc magnetic field. The case treated, pictured in Fig. 1, is that of a p-polarized TEM wave, obliquely incident on a uniform plasma whose dc magnetic field (when present) is taken to aligned both perpendicular to the density gradient and the plane of wave incidence. The analyses pertain to both $k_0 l > 1$ and $k_0 l < 1$, where k_0 is the free-space wave number and $l = n_e / |\nabla n_e|$, is the scale length on which the plasma density varies. We assume that the ions are at rest with an assigned density distribution and take the field quantities to be a sum of a static part and a small high-frequency part, the latter being treated by linearized equations.

Expressions for the linear current densities in an inhomogeneous plasma in the presence of a static magnetic field have been derived by Bernstein and Weenink, by Pearson, by Baldwin, by Azevedo and Vianna, and by Sivasubramanian and Tang.[5-9] Generally, these expressions describe the effects of electric fields and particle drifts within plasma and include the effect of an electrostatic field balancing the plasma nonuniformity as well as the anisotropy of the unperturbed electron-velocity distribution function. These equations when substituted into Maxwell's equations allow us to study the electromagnetic and plasma fields everywhere within the hot plasma with or without consideration of collisions.

In this paper I describe the numerical solutions for the complex electric and magnetic fields, electron flow, electron resonant heating, and dc magnetic field generation within the plasma as well as the absorption and reflection of the incident TEM wave. I also investigate the dependence of each of the above quantities on angle of incidence in the range −60 to +60 deg. My conclusions are given in the final section.

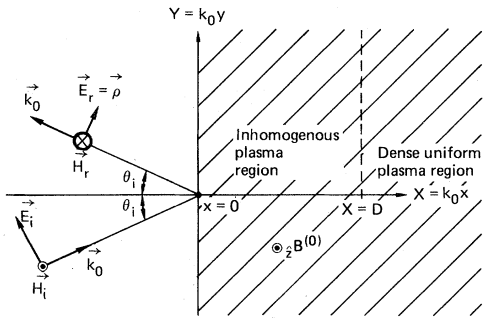

FIG. 1. p-polarized electromagnetic fields incident on and reflected from an inhomogeneous plasma.

BASIC FORMULATION

In the high-power pulsed electromagnetic-wave–plasma interaction problem, two time scales are evident, namely, the time τ associated with the pulse duration and a shorter time ω^{-1} corresponding to the radiation period. To obtain a fluid description valid on the longer time scale, it is useful to average the effects due to a high-frequency phenomena by taking a time average $\langle\ \rangle \equiv T^{-1}\int_{-T/2}^{T/2} dt$, where $\omega^{-1} \ll T \ll \tau$. Various quantities in the plasma can then be treated in terms of a dc and high-frequency part, e.g., $\vec{f} = (\vec{f}^{(0)} + \langle \vec{f} \rangle) + \vec{f}^{(1)}$, etc. The superscript zero refers to an equilibrium quantity while the superscript one refers to a first-order quantity for which we assume a time dependence $\exp(-i\omega t)$.

My model is based on the full set of Maxwell's equations and the moments of the Boltzmann equation. Maxwell's equations are

$$\nabla \times \vec{E} = -\mu_0 \frac{\partial \vec{H}}{\partial t}, \tag{1a}$$

$$\nabla \times \vec{H} = \vec{j} + \epsilon_0 \frac{\partial \vec{E}}{\partial t}, \tag{1b}$$

$$\epsilon_0 \nabla \cdot \vec{E} = \rho, \tag{1c}$$

$$\mu_0 \nabla \cdot \vec{H} = 0, \tag{1d}$$

where $\vec{j} = n_0 q \vec{v}$ and $\rho = n_0 q$ are the current and charge densities, respectively. Equations (1) imply the continuity law

$$\left(\frac{\partial}{\partial t}\right) n_0 m + \nabla \cdot (n_0 m \vec{v}) = 0, \tag{2}$$

while conservation of momentum dictates

$$m n_0 \frac{\partial}{\partial t} \vec{v} = \vec{f}, \tag{3}$$

where the thermokinetic and first-order Lorentz-force density components of $\vec{f}$ are

$$\vec{f}_T = -\nabla \cdot \underline{P}, \tag{4a}$$

$$\vec{f}^{(1)} = -e n_e (\vec{E}^{(1)} + \vec{v}^{(1)} \times \vec{B}^{(0)}), \tag{4b}$$

with thermokinetic tensor $\underline{P}$. The time-averaged (ponderomotive) force component of $\vec{f}$ is given by[10]

$$\langle \vec{f} \rangle = \nabla \cdot \underline{P}_R, \tag{5}$$

where the radiation pressure is

$$\underline{P}_R = -\epsilon_0 [\langle \epsilon \vec{E}^{(1)} \vec{E}^{(1)} \rangle + \langle \vec{B}^{(1)} \vec{B}^{(1)} \rangle] + \underline{I} \tfrac{1}{2} \epsilon_0 [\langle E^{(1)2} \rangle + \langle B^{(1)2} \rangle],$$

where $\epsilon = 1 - \omega_p^2/\omega^2$.

The time rate of power absorption is calculated through the use of the energy conservation theorem

$$\frac{\partial}{\partial t} \frac{1}{2} n_e m \langle v^2 \rangle_{x,t} = \langle \vec{j} \cdot \vec{E} \rangle_t + \frac{\partial}{\partial t} (\tfrac{3}{2} n_e \kappa T)\Big|_{\text{coll+cond}} \tag{6}$$

for an electron temperature $\frac{3}{2}\kappa T_e = \langle \frac{1}{2} m v^2 \rangle_x$. Equation (6) is valid if the kinetic energy gained by the electrons is less than mc^2; relativistic corrections must be included when this is not the case.

LINEAR CURRENT DENSITY

The linear first-order current density is given by[6,7]

$$\frac{\vec{j}^{(1)}}{i\omega\epsilon_0} = a(\vec{E} - i\Omega \vec{E} \times \hat{z}) + \frac{c^2}{\omega^2}\{\delta \nabla [a(\nabla \cdot \vec{E} - 2i\Omega \hat{z} \cdot \nabla \times \vec{E})] + \delta \hat{z} \times \nabla [a(\hat{z} \cdot \nabla \times E + 2i\Omega \nabla \cdot \vec{E})] - 2\delta \hat{z} \times \nabla a \cdot \nabla (\vec{E} \times \hat{z} + 2i\Omega \vec{E}) + \hat{z} \times \nabla (\Delta \hat{z} \cdot \nabla \times \vec{E})\}, \tag{7}$$

where

$$a = \omega_p^2(x)/\omega^2(1 - \Omega^2), \quad \delta = -3\langle v_x^2 \rangle_x / c^2,$$
$$\Delta = 2\langle v_x^2 \rangle_x a / 3c^2, \quad \Omega = \omega_c/\omega.$$

The zero-order magnetic field is $\vec{B}^{(0)} = \hat{z} B_0$, and the local electron-plasma frequency is $\omega_p(x) = [n_e(x) e^2/m\epsilon_0]^{1/2}$. Equation (7) has been derived under the assumption that the electron density is large enough so that the Debye length $\lambda_D \ll l$. Ad-

ditionally, in Pearson's derivation,[6] we require $B^{(0)}$ to be strong enough so that the electric field and density variation are small over a Larmor radius. On the other hand, Baldwin[7] has shown that the expansion parameter in the derivation of Eq. (7) can be either r_L/l or $\langle v_x^2 \rangle_x^{1/2}/\omega l$, where r_L is the Larmor radius and $\langle v_x^2 \rangle_x$ is the mean-square x-directed thermal velocity. Thus Eq. (7) is equally valid in the limit $\omega_c = -eB^{(0)}/m \to 0$. As discussed in Ref. 7, the inclusion of Landau damping in Eq. (7) requires a more generalized treatment.

With reference to Fig. 1, we assume an electromagnetic field to be obliquely incident on the plasma at $X = k_0 x = 0$. We assume the plasma to be inhomogeneous along the x direction and take the perturbation quantities to depend spatially only on x. The y dependence is taken to be $\exp(ik_y y) = \exp(in Y)$, where $n = k_y/k_0 = \sin\theta_i$, θ_i is the angle of incidence, and $Y = k_0 y$. Table I gives the notation used in this paper as well as values for the scaling parameters.

In a Cartesian coordinate frame, Eq. (7) can be written as

$$\frac{j_x^{(1)}(x,y)}{i\omega\epsilon_0} = a\delta E_x'' + a'\delta E_x' + (a - n^2 a\delta + 2\Omega n a'\delta)E_x - 2i\Omega a\delta E_y'' - 2i\Omega a'\delta E_y' - i(\Omega a - n a'\delta)E_y \tag{8a}$$

and

$$\frac{j_y^{(1)}(x,y)}{i\omega\epsilon_0} = a\delta E_y'' + a'\delta E_y' + (a - n^2 a\delta + 2\Omega n a'\delta)E_y + 2i\Omega a\delta E_x'' - 2i\Omega a'\delta E_x' + i(\Omega a + n a'\delta)E_x , \tag{8b}$$

where the primes denote differentiation with respect to the parameter X.

NONLINEAR CURRENT DENSITY

The nonlinear current density, the source for many effects observed in plasma irradiated by strong electromagnetic waves, can be derived

TABLE I. Notation and numerical parameters used in text and figures.

Parameter	Symbol and formula	Value or comment
Normalized spatial parameter	$X = k_0 x$	
Source wavelength	$\lambda_0 = 1.06\ \mu$	
Debye length at critical density	$\lambda_{DE} \approx 0.02\ \mu$	
Source wave number	$k_0 = 5.93 \times 10^6 \mathrm{m}^{-1}$	
Source frequency	$\omega = 1.77 \times 10^{15} \mathrm{rad/sec}$	
Normalized density factor	$a = \omega_p^2/(\omega^2 - \omega_c^2)$	
Local density gradient	$a' = (\omega^2 - \omega_c^2)^{-1} d\omega_p^2/dX$	
Normalized temperature parameter	$\delta = -3\langle v_x^2 \rangle / c^2$	
Normalized scale length	$L = k_0 l = k_0 (\nabla n_e/n_e)^{-1} = a/a'$	
Upper hybrid resonance (critical density)	X_0, $(a = 1)$	
Sine of angle of incidence	$n = \sin\theta_i$	
Time average (slow time scale of a quantity u)	$\langle u \rangle_t$	
Spatial average (over electrostatic-field oscillation frequency) of a quantity u	$\langle u \rangle_x$	
Irradiance	$I_0 = \epsilon_0 c \frac{1}{2} E_0^2$	$10^{15}\ \mathrm{W/cm^2}$, $2 \times 10^{16}\ \mathrm{W/cm^2}$
Incident-field strength	E_0	$8.7 \times 10^{10} \mathrm{V/m}$, $4 \times 10^{11} \mathrm{V/m}$
Mean-square x-directed thermal velocity	$\langle v_x^2 \rangle^{1/2}$	$\sim 3 \times 10^7 \mathrm{m/sec}$
Small-magnetic-field expansion parameter	$v/\omega l$	$\sim 6 \times 10^{-3}$
Quivering velocity	$v_E^{(1)} = \lvert eE_0/m_e\omega \rvert = 0.25\lambda_0\sqrt{I_0}\ \mathrm{msec}^{-1}$, $\lambda_0\ (\mu)$, $I_0\ (\mathrm{W/cm^2})$	$(v_E/c \approx 0.13)$
Thermal velocity	$v_T = (\kappa T_e/m_e)^{1/2} = 1.3 \times 10^7 \sqrt{T_{\mathrm{keV}}}\ \mathrm{msec}^{-1}$	$(v_T/c \approx 0.1)$
Field-strength parameter	$\eta = v_E/v_T = 1.9 \times 10^{-8} \lambda_0 (I_0/T_{\mathrm{keV}})^{1/2}$	$\sim 0.3 \to 1.3$

from the ponderomotive-force description. We rewrite Eq. (5) as

$$\langle \vec{f} \rangle = (\epsilon_0/\mu_0)^{1/2} \langle \vec{j} \times \vec{\mathcal{H}}_z \rangle - \langle \epsilon_0 a \vec{E} \cdot \nabla \vec{E} \rangle , \tag{9}$$

where $\mathcal{H}_z \equiv (\mu_0/\epsilon_0)^{1/2} H_z = -iE_y' - nE_x$ follows from Faraday's law [Eq. (1a)]. (Some controversy remains in the fluid and kinetic descriptions as to which terms the gradient operator operates on.[11,12] Hora[12] finds, in our notation

$$\langle f \rangle \approx (\epsilon_0 \mu_0)^{1/2} \langle j \times \mathcal{H}_z \rangle - \langle \epsilon_0 a \vec{E} \cdot \nabla E + \epsilon_0 (1-a) E \nabla \cdot E - \epsilon_0 \vec{E}\vec{E} \cdot \nabla a \rangle . \tag{10}$$

I have investigated numerical results using both representations [Eq. (9) and (10)] and find only slight waveform modification for the density gradients in this paper. The calculations presented here are those using Eq. (9), which yields currents [Eq. (12)] identical to those in a region of validity of the Poisson approximation [Eq. (13)].)

Equation (9) may be reduced to x- and y-component form:

$$\langle f_x \rangle = k_0 \epsilon_0 a \langle -E_x E_x' - inE_y E_x \rangle + \mathcal{O}(n) + \mathcal{O}(\delta) ,$$

$$\langle f_y \rangle = k_0 \epsilon_0 a \langle -E_x E_y' - inE_y^2 \rangle + \mathcal{O}(n) + \mathcal{O}(\delta) , \tag{11}$$

leading to the induced currents

$$\frac{\langle j_x \rangle}{i\omega\epsilon_0} = \frac{-ek_0}{\omega^2 m} a \langle E_x E_x' + inE_x E_y \rangle + \mathcal{O}(\delta) , \tag{12a}$$

$$\frac{\langle j_y \rangle}{i\omega\epsilon_0} = \frac{-ek_0}{\omega^2 m} a \langle E_x E_y' + inE_y^2 \rangle + \mathcal{O}(\delta) . \tag{12b}$$

Similar expressions for the nonlinear current density may be obtained by substituting Poisson's law into the current density, yielding

$$\langle \vec{j} \rangle = \rho \langle \vec{v} \rangle = \langle (\epsilon_0 \nabla \cdot \vec{E}) \vec{v} \rangle \approx i \frac{\epsilon_0 q}{\omega m} \langle (\nabla \cdot \vec{E}) \vec{E} \rangle \tag{13a}$$

or

$$\frac{\langle j_x \rangle}{i\omega\epsilon_0} = \frac{-ek_0}{\omega^2 m} \langle E_x E_x' + inE_x E_y \rangle , \tag{13b}$$

$$\frac{\langle j_y \rangle}{i\omega\epsilon_0} = \frac{-ek_0}{\omega^2 m} \langle E_x' E_y + inE_y^2 \rangle . \tag{13c}$$

In each of the above derivations, the nonlinear current density is determined by the iterative procedure of initially solving for the first-order field quantities.

WAVE EQUATIONS

Since $\vec{E}$ is taken to be composed of both slow and fast (harmonic) time scales associated with incident-wave pulse length and frequency, a high-frequency wave equation for the electric field follows from Eq. (1),

$$\nabla \times \nabla \times \vec{E} - \frac{\omega^2}{c^2} \vec{E} - 2i \frac{\omega}{c^2} \frac{\partial}{\partial t} \vec{E} = -\frac{\omega^2}{c^2} \frac{\vec{j}}{i\omega\epsilon_0} . \tag{14}$$

Substitution of Eq. (8) into (14) yields

$$\frac{2i}{\omega} \frac{\partial}{\partial t} \begin{pmatrix} E_x \\ E_y \end{pmatrix} = \underline{L} \begin{pmatrix} E_x \\ E_y \end{pmatrix} , \tag{15}$$

where the elements of the operator $\underline{L}$ are given approximately by

$$L_{11} = a\delta\nabla_x^2 + a'\delta\nabla_x + a - 1 + n^2 + 2\Omega n a'\delta ,$$

$$L_{21} = L_{12}^* = i2\Omega a\delta\nabla_x^2 + i(2\Omega a'\delta + n)\nabla_x + i(\Omega a + na'\delta) ,$$

$$L_{22} = -\nabla_x^2 + a'\delta\nabla_x + a - 1 + 2\Omega n a'\delta .$$

Equation (15) is similar to that used in a hybrid numerical-simulation study.[13] In the steady state, the high-frequency fields $E_{x,y}$ may be obtained in the following way: We combine Eq. (15) into a single fourth-order differential equation for E_y. Expressions for the fields E_y and $\mathcal{H}_z$ can then be obtained by matching external tangential fields to the solutions of this differential equation at the boundaries. The electric field E_x can then be recovered with the use of Faraday's law $\nabla \times \vec{E} = i\omega\mu_0 \vec{H}$. Setting the left-hand side of Eq. (15) to zero, we find[14]

$$AE_y^{IV} + BE_y''' + CE_y'' + DE_y' + FE_y = 0 , \tag{16}$$

where

$$A = 1 + \varphi n^2 (a - 1 + n^2) ,$$

$$B = -\frac{a'}{a} \frac{a+2}{a-2} + \varphi n^2 \frac{a'}{a} (a - 2 + 2n^2) ,$$

$$C = p^2 A + \text{hybrid resonance terms} ,$$

$$D = -(a'/a)(a-2) + \varphi n^4 (a'/a\delta) ,$$

$$F = p^2 q^2 + \varphi n^2 \left(p^2 (q^2 - n^2)(a - 1 + n^2) - n \frac{(\omega_c/\omega) a'}{a\delta} (1 - n^2) \right) ,$$

$$\varphi = [a\delta (a-2)^2 \omega_c^2/\omega^2]^{-1} ,$$

and the hybrid resonance terms are approximately equal to

$$a'^2 \left(3 - \frac{n^2}{\delta} \frac{\omega^2}{\omega_c^2} \right) + a'' \left(1 + \frac{n^4}{\delta} \frac{\omega^2}{\omega_c^2} \right) .$$

The quantities p and q are given by

$$p^2 = \frac{a-1}{a\delta} = \frac{c^2 (\omega_p^2 - \omega^2 + \omega_c^2)(4\omega_c^2 - \omega^2)}{3\langle v_x^2 \rangle_x \omega^2 \omega_p^2} , \tag{17}$$

$$q^2 = \frac{(a\omega_c/\omega)^2 - (a-1)^2}{a-1} = -\frac{[\omega_p^2 - \omega(\omega + \omega_c)][\omega_p^2 - \omega(\omega - \omega_c)]}{\omega^2 (\omega_p^2 - \omega^2 + \omega_c^2)} \tag{18}$$

and represent the refractive indices of the plasma and electromagnetic waves, respectively.

Away from the critical density, Eq. (16) can be decoupled into two second-order homogeneous (nonforced) equations. Ignoring terms of $\mathcal{O}(\delta)$ with respect to unity, while making use of Faraday's law, we recover[15]

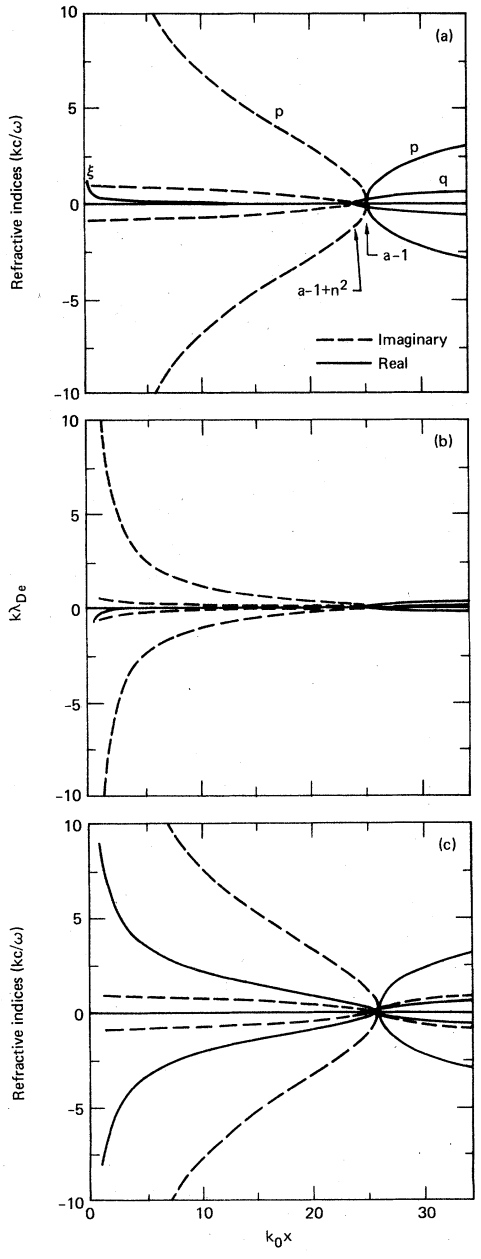

FIG. 2. Refractive indices vs k_0x for an inhomogeneous plasma having a ramp profile with $k_0l=26$, $T_e=5.1$ keV, $\omega/\omega_c=100$, and $\theta_i=11$ deg: (a) and (b), $\nu_q=\nu_p=0$; (c) $\nu_q=0$, $\nu_p=0.6\omega$.

$$E_x''+\frac{a'}{a}E_x'+p^2E_x=0\,, \tag{19}$$

$$\mathcal{H}_z''+\frac{a'}{1-a}\mathcal{H}_z'+(q^2-n^2)\mathcal{H}_z=0\,. \tag{20}$$

Equation (19) describes longitudinal plasma waves, while Eq. (20) describes the electromagnetic cold-plasma field, as can be verified by setting $\langle v_x^2\rangle$ equal to zero in the previous formulation. Equation (20) has been previously used to study resonant absorption of obliquely incident laser light.[16] This was accomplished numerically by introducing a phenomenological collision frequency, which removes the cold-plasma singularity associated with the $\mathcal{H}_z'$ coefficient by displacing it off of the real axis in the complex-x plane. However, at the singularity $a=1$, Eq. (20) is invalid and Eq. (16) must be used in its entirety.

The nature of the wave solutions at hand is illustrated in Fig. 2. The real and imaginary roots of Eq. (16) can be identified as the refractive indices p and q. Here $k_0l=26$, $T_e=5.1$ keV, and $\theta_i=11$ deg. The damping increment is ξ, a consequence of the kinetic theory.[17] Thus for the collisionless case, right- and left-propagating q waves connect to damped q fields at the turning point $a=1-n^2$. To the right of the singularity $a=1$, only damped p and q waves exist. The root modification and increased damping due to collisions is shown in Fig. 2(c).

NUMERICAL SOLUTION

In this section we describe QUELLE, a code that solves for the electric and magnetic fields, current densities, energy flux, reflection, transmission, and absorption of an electromagnetic field of arbitrary wavelength obliquely incident on a planar inhomogeneous plasma.[14] The code numerically integrates (by the implicit Adams method with functional iteration) the complete set of coupled-wave equations with suitable initial and boundary conditions.

For simplicity, we start our calculation at $x=D$, where the solutions of E_x and E_y consist of a linear combination of four damped waves, two of which can be identified, initially, as longitudinal p waves and the other two as electromagnetic q waves. We decompose the right-hand side of Eq. (15) into 32 first-order differential equations (16 real and 16 imaginary) and initiate independent solutions by use of the Kronecker initial conditions.

To numerically calculate the general solutions E_x and E_y within the plasma, it is necessary to determine four arbitrary constants associated with four independent solutions. These four constants plus an additional two representing the reflection

coefficient at $X=0$ and the transmission coefficient at $X=D$ must be found by using six boundary conditions to match the incident, reflected, and transmitted fields to a linear combination of independent solutions.

Continuity of E_y and $\mathcal{H}_z \propto dE/dx$ across the plasma boundary provides two of the boundary conditions at $X=0$. For the third boundary condition we use a method based upon the continuity of the displacement suggested by Bernstein and Weenink.[5] We assume the conditions that the scale length in the equilibrium sheath, which provides for the containment of the particles at the edge of the plasma, is small compared to the length of the perturbation quantities but large compared to a radius r described below. Thus we require the condition

$$k_0 r \ll \Delta X \ll |p^{-1}| \tag{21}$$

in the sheath region, where r is either r_L (strong-magnetic-field limit) or v_{th}/ω (weak-magnetic-field limit) and $\Delta X = X_2 - X_1 \approx a/a'$ is the width of the density discontinuity (sheath thickness). These conditions insure that Eq. (7) is valid throughout ΔX. The assumption given by the left-hand side of the above inequality is clearly violated for a uniform plasma or a plasma with sharp boundaries. In deriving Eq. (21), we have used the fact that the fastest variation of the perturbation electric field is roughly that of the longitudinal waves with associated refractive index p. If Eq. (21) holds for the longitudinal field, it is necessarily satisfied by the electromagnetic field.

Following Baldwin,[7] we can now integrate either the pair of Maxwell's equations or, equivalently, the coupled-wave equations (15) over a thin disk lying in the boundary surface. Within this thin plasma layer, the physical quantities are assumed to change continuously. This integration is carried out in the Appendix. We find the third boundary condition to be continuity of the parameter

$$\Gamma \equiv (a\delta[E_x' - iE_y' + n(E_x - iE_y)])_{x_1}^{x_2} = 0$$

across $X=0$. Note that when $n=\sin\theta_i=0$, this boundary condition reduces to that used by Bernstein and Weenink[5] for the case of normal wave incidence. The remaining three boundary conditions at $X=D$, which connect the region of large density gradient with a quasiuniform plasma region, are simply taken to be the continuity of the tangential fields E_y and $\mathcal{H}_z$ with E_x set equal to 0.

In the remainder of this paper, the density gradient is initially taken to be linear, with the critical density located at either $X_0=11$ or $X_0=26$. The incident wavelength is taken to be $\lambda_0=1.06\ \mu$, and the plasma electron temperature is either 4 or 5.1 keV. These values have been chosen so that selected snapshots of the fields can be directly compared to known simulation code predictions.

ELECTRIC AND MAGNETIC FIELDS

Figure 3 illustrates the complex fields E_x, E_y, and $\mathcal{H}_z$ for $v_E/v_T \ll 1$ and $v_E/v_T > 1$ ($I_0 = 10^{16}$ W/cm^2). The turn-on fields depicted in Fig. 3(a) show $E_x/E_0 \gg 1$ and are the linear fields initially present at the start of some applied pulse or cw wave when I_0 is small. The largely cold-plasma E_y and $\mathcal{H}_z$ fields of Fig. 3(b), uncoupled from the hot-plasma longitudinal fields as a result of efficient absorption, are seen to display the same characteristics found by Friedberg *et al.*[16]

Particle collisions have been included in the preceeding formulation in the following way. Associated with the cold-plasma permittivity $\epsilon = 1 - a$

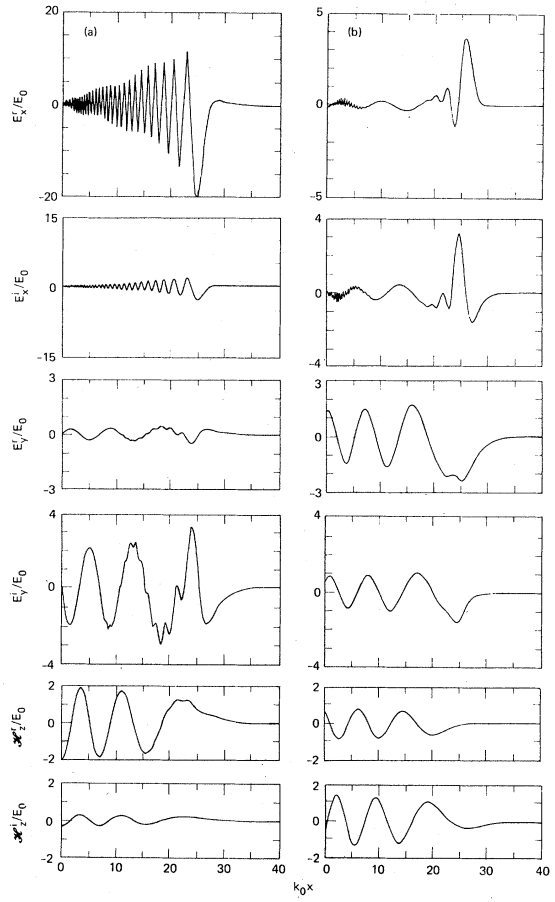

FIG. 3. Complex fields E_x/E_0, E_y/E_0, and $\mathcal{H}_z/E_0$ vs k_0x for $k_0l=26$, $T_e=5.1$ keV, $\omega/\omega_c=100$, and $\theta_i=11$ deg: (a) collisionless case, (b) $\nu_p=0.6\omega$, $\nu_q=\nu_{ei}$. The noise in E_x for small k_0x results from underdamped plasma waves.

is a fast-wave collision frequency ν_q ($\omega \to \omega + i\nu_q$) so that $a \to a_r + ia_i$. We take the average electron-ion collision frequency to be

$$\frac{\nu_q}{\omega} = \left\langle \frac{\nu_{ei}}{\omega} \right\rangle_x = \left(\frac{2a}{\pi}\right)^{1/2} \frac{\ln \Lambda}{\Lambda} , \tag{22}$$

where $\Lambda = 12\pi n_e \lambda_{De}^{-3}$. To discuss energy absorption resulting from the slow waves, we must consider the effect of turbulence, which will produce an increased effective electron collision frequency $\nu_{eff} = \nu_p$. This second collision frequency is entered into the formulation $\omega \to \omega + i\nu_p$ through the electron temperature term $\delta \to \delta_r + i\delta_i$. Appropriate to the problem considered here are intensity-dependent collision models.[18-20] We take[19]

$$\frac{\nu_{eff}}{\omega} = \tfrac{1}{2} a^{1/2} \frac{\omega_a}{\nu_a} \frac{\epsilon_0 E_x^2}{2 n_e \kappa T_e} , \tag{23}$$

where ω_a and ν_a are the ion-acoustic rotational and collisional frequencies, respectively. For the case of critically damped acoustic waves, Eq. (23) yields $\nu_{eff}/\omega = 0.66$ at the upper hybrid resonance for $I_0 = 2.2 \times 10^{16}$ W/cm^2. In comparison, another model gives[20]

$$\frac{\nu_{eff}}{\omega} = a^{1/2} \left(\Phi \frac{\epsilon_0 E_x^2}{n_e \kappa T_e}\right)^{1/2} (2\pi k_0 l)^{-1/4} (k\lambda_{De})^{1/2} . \tag{24}$$

Here we replace the Denisov parameter[21] Φ (derived for $k_0 l \gg 1$) with $(\pi A)^{1/2}$, where the absorption A is that obtained from the following sections. At maximum field absorption (A is known[14] to depend only weakly on T_e), Eq. (24) yields $\nu_{eff}/\omega \approx 0.2$ at $a = 1$. A best fit between QUELLE and simulations is found to occur when $\nu_p/\omega \approx 0.6$, that is, when the irradiance lies in the range 1–2 $\times 10^{16}$ W/cm^2. Of course, in any experimental situation, it would be good to have a specification of the effective charge number $\bar{Z}$ as a function of spatial coordinate in the collisional representation.

CURRENT FLOW

The two-dimensional current flow associated with Fig. 3(b) is illustrated in Fig. 4. The electron flow, opposite the current flow, is most rapid through the upper hybrid resonance where it is seen to be canted somewhat to the x direction. This current density indicates that the plasma electrons are accelerated in the direction of decreasing density owing to the force density when the wave frequency of the incident TEM field is much greater than the cyclotron frequency.

INDUCED MAGNETIC FIELDS

An important phenomenon observed in simulation studies is the generation of a MG dc magnetic field, a topic that has received considerable interest.[22-29] (The numerical work of W. Woo *et al.* has also shown this phenomenon.[30,31]) The source of this field can be traced to the time-averaged y-directed nonlinear current density. From Ampere's law it follows that

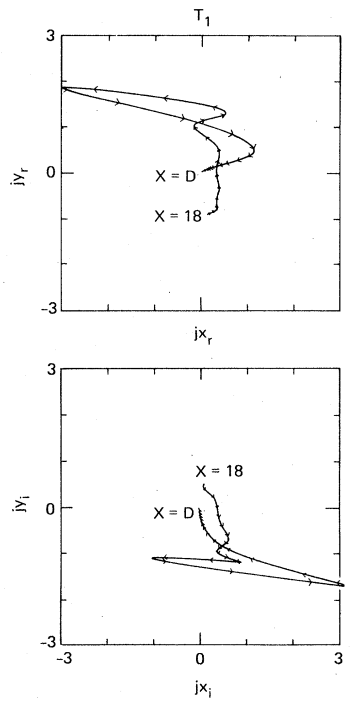

FIG. 4. Complex current flow in inhomogeneous plasmas. (Electron motion is opposite to arrows.) Parameter values are the same as in Fig. 3(b).

$$\hat{x} i n \langle B_z \rangle - \hat{y} \frac{\partial}{\partial x} \langle B_z \rangle = \frac{\mu_0}{k_0} \langle \vec{j} \rangle . \tag{25}$$

Thus $\langle B_z \rangle$ can be determined once $\vec{j}$ is specified. Substituting Eq. (12b) into the y component of Eq. (25) while ignoring terms of order $\mathcal{O}(n, \omega_c, \delta)$, we find

$$\langle B_z \rangle = (e\mu_0\epsilon_0/m\omega) a \langle i E_x E_y \rangle . \tag{26}$$

[Analytic solution of Eq. (16) shows that, in the vicinity of the upper hybrid resonance, Eq. (26) can be broken down into a simple form

$$\langle B_z \rangle \approx -(e\mu_0\epsilon_0/2m\omega) a E_{y_i}^{EM} E_{x_r}^{L} , \tag{27}$$

where $E_{y_i}^{EM}$ is the imaginary cold-plasma y-directed electromagnetic field and $E_{x_r}^{L}$ is the real x-directed longitudinal field, which is finite for $\theta_i = 0$ only if $B^{(0)} \neq 0$. The separation of the longitudinal and electromagnetic field components is not possible in simulations or the numerical treatment.]

Figure 5 illustrates $\langle B_z \rangle$ vs $B^{(0)}$ as a function of Θ_i for $I_0 = 10^{16}$ W/cm^2. Figure 6 compares $\langle E_x E_y \rangle / E_0^2$ and $\langle B_z \rangle$ derived from this theory to

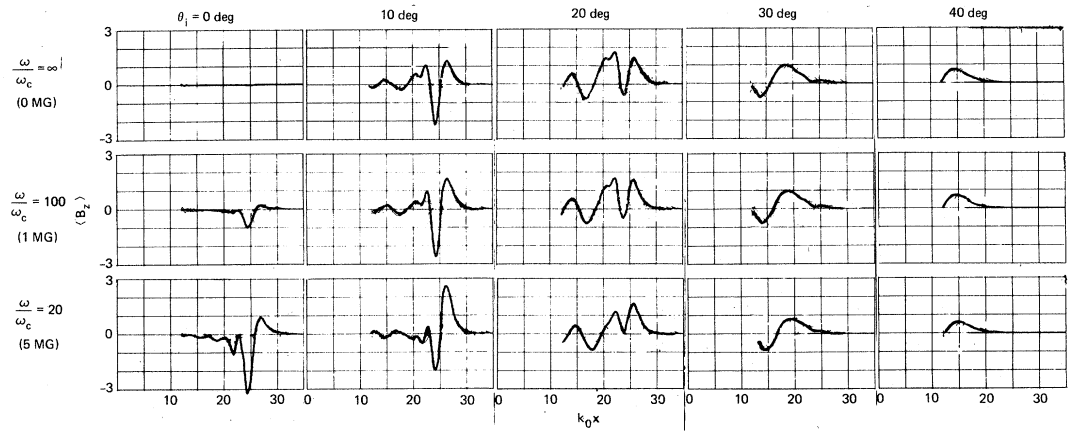

FIG. 5. Time-averaged magnetic field $\langle B_z \rangle$ vs $B^{(0)}$ and θ_i for $I_0 = 10^{16}$ W/cm^2. Parameter values are the same as in Fig. 3(b).

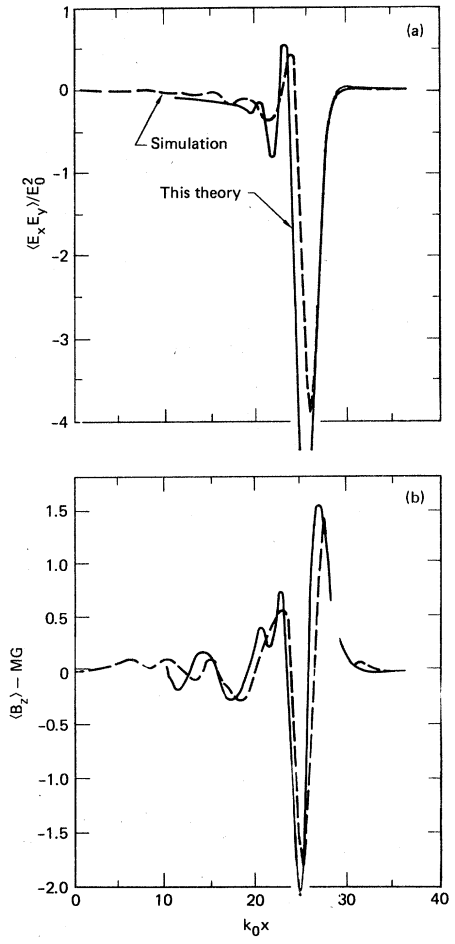

FIG. 6. Variation of $\langle E_x E_y \rangle / E_0^2$ and $\langle B_z \rangle$ The simulation results are for $\omega_0 t = 162$, and the results of this theory are for $k_0 l = 26$, $T_e = 5.1$ keV, $\omega/\omega_c = 100$, and $I_0 = 2.2 \times 10^{16}$ W/cm^2.

calculations from the relativistic $2\frac{1}{2}$-dimensional particle simulation code ZOHAR.[25] I have found these fields to be excited even after the electromagnetic wave has tunneled through an overdense plasma of thickness $X = 20$ and again reached a critical layer (as could occur when a mirror image is connected to the geometry under consideration). Thus we expect that in an experimental situation "spontaneous" generation of magnetic fields should occur even when only a very weak wave of length λ_0 is present.

ABSORPTION AND REFLECTION OF THE INCIDENT FIELD

Associated with the fields derived in the previous sections is the reflectivity ρ, transmissivity τ, and power absorptivity $A = 1 - |\rho|^2 - |\tau|^2$. Figure 7 illustrates the evolution of A with θ_i and field strength $B^{(0)}$. The effect of a finite $B^{(0)}$ is to convert the incident electromagnetic field into an extraordinary field within the plasma. This provides for an excitation field E_x when $\theta_i = 0$ and E_x is the source for absorption of normally incident fields. The case of zero absorption now occurs at some negative angle of incidence. Figure 8(a) shows zero absorption at −10 deg for a 5-MG, $L = 26$ plasma. The large absorption occurring at +8 deg is contrasted by a maximum absorption of only 10% for negative angles of incidence. The lack of absorption symmetry with θ_i is a consequence of asymmetrical terms ($n = \sin\theta_i$) in the current density equation (7).[14] In Fig 8(b) the dots represent simulation calculations at late time. Thus, for the parameters used here, we can estimate that about 3 to 5% of the absorbed light at $\theta_i = 0$ results from resonant absorption in a magnetized plasma. The remainder can be attributed

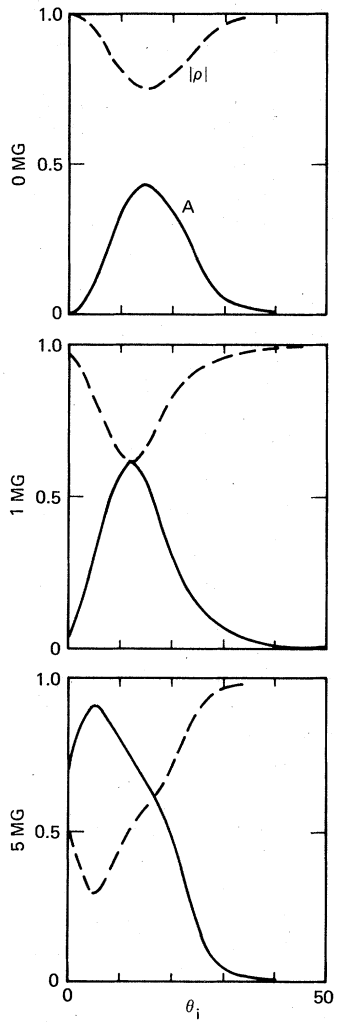

FIG. 7. Evolution of the absorption A and reflectivity $|\rho|$ vs positive angles of incidence. Parameter values are the same as in Fig. 3(b).

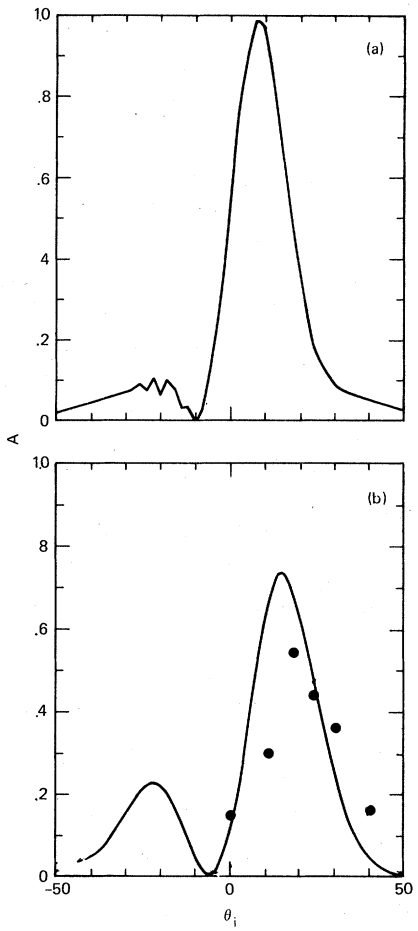

FIG. 8. Absorption vs positive and negative angles of incidence: (a) $k_0 l = 26$, $T_e = 5.1$ keV, $B^{(0)} = 5$ MG; (b) $k_0 l = 11$, $T_e = 4$ keV, $B^{(0)} = 4$ MG. Dots represent late-time simulation results.

to the generation of ion-acoustic waves, leading to Brillouin backscatter. The calculated magnitude and phase of the wave reflectivity, necessary for the design of any focusing-diagnostics system for laser light, is given in Fig. 9.

KINETIC ENERGY OF RESONANT ELECTRONS

The conversion of the extraordinary field into a slow electrostatic wave is the mechanism whereby electrons resonant with this wave acquire momentum and energy. The energy gained by the electrons, which in steady state attain a temperature higher than the field-free equilibrium value, is equal to that lost in collisions with ions and in thermal conduction. To correctly calculate the increase in temperature T_e requires the simultaneous solution of Eqs. (3) and (6), which requires knowledge of the thermal conductivity[32] or diffusivity.[33] I do not solve this complete problem, but we can determine the kinetic energy gained by resonant electrons by using the first term on the right-hand side of Eq. (6), which in steady state yields

$$T_{\mathrm{KE}} = T_0 + e^2 |\vec{\mathrm{E}}|^2 / m_e \omega^2 ,$$

where T_0 is the equilibrium temperature of the plasma (a relativistic derivation is appropriate when the kinetic energy is of the order of or greater than the rest energy[34]). Figure 10 depicts this coherent electron energy. These oscillations can be viewed as a source for plasma heating. In a one-dimensional, two-temperature hydrodynamics code, the deposition of local energy corresponding to that calculated here yields increased, spatially varying electron and ion temperatures in the underdense region.[33]

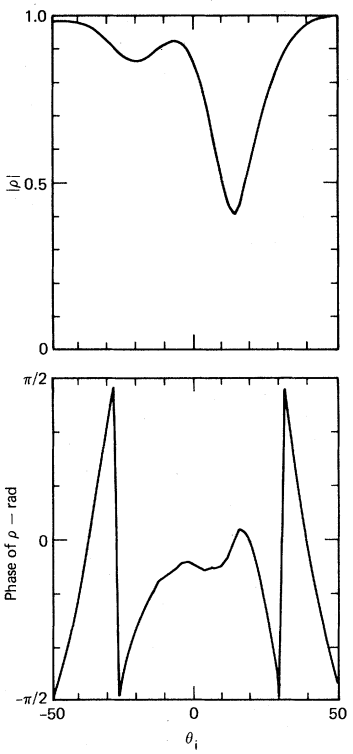

FIG. 9. Magnitude and phase of reflectivity ρ vs positive and negative angles of incidence. Parameter values are the same as in Fig. 3(b).

CONCLUSIONS

The theory presented here is based on a kinetic current-density treatment, the full set of Maxwell's equations, and moments of the Boltzmann equation and accounts for the behavior of plasma irradiated by intense, or weak, obliquely incident electromagnetic waves. An investigation of the plasma-wave excitation and subsequent absorption has been carried out here by examining the relation between field-strength-dependent collision frequencies. The dc magnetic field generation quantitatively shows close agreement to simulations (Fig. 6). The dc magnetic field, whose characteristic profile with position x is determined by a beating along the density gradient, between the hot-plasma longitudinal field and cold-plasma transverse field, results from the nonlinear current density j_y. The acceleration of electrons to less-dense regions (Fig. 4) and the decrease in the energy carried by the hot-plasma resonant electrons as the density gradient becomes larger with time verifies simulation predictions.

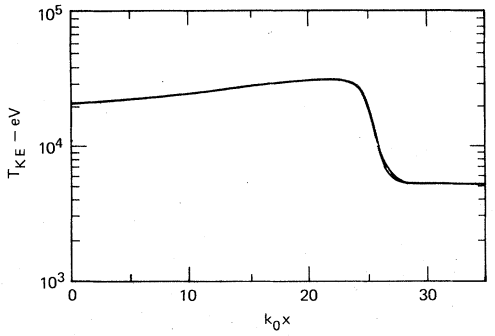

FIG. 10. Kinetic energy gained by resonant electrons. Initial plasma values are: $k_0 l = 26$, $T_e = 5$ keV, $B^{(0)} = 1$ MG, $\nu_a = \nu_p = \langle \nu_{ei} \rangle$.

The presence of a MG level dc magnetic field in plasma for which T_e is a few keV and $k_0 l \approx 1$–30 introduces an asymmetry, with respect to angle of incidence, in the absorption of incident wave power. An increase in absorption occurs for positive angles while a decrease is observed for negative angles. The case of zero absorption is shifted from 0 deg to some negative angle when a z-directed dc magnetic field is present (Fig. 8). The magnitude and phase of the reflected laser light (Fig. 9) should reveal useful information about the absorption process and internal plasma parameters.

An example of the utility of the analytical-numerical theory in investigating, in detail, wave-plasma interaction problems as well as unfolding the physical mechanisms responsible for observed phenomena is given by the data depicted in Fig. 6. Here the simulation required a time expenditure of 180 min on a CDC 7600 computer,[35] while the numerical treatment required 5 sec. Additionally, the direct comparison of a nonsimulation prediction to a simulation result verifies the validity of several assumptions made in both approaches.

I believe the model could be improved by including ion motion, arbitrarily directed magnetic fields, and harmonic generation. Closely related to the problem of longitudinal-wave excitation and absorption at the critical density is the nonlinear mixing of waves in inhomogeneous plasma. Current-density expressions for this mixing have been derived,[36] and such effects have been seen in simulations.[37] Absorption in nonplanar geometries would be another valuable addition to the model. Here I have considered a planar geometry, but the formulation is applicable to problems having cylindrical or spherical geometries. The model would also benefit from including nonuniform plane-wave analysis. In experimental situations where a beam is focused on a target, a superposition of plane waves is a better representation of the incident radiation. Although such an analysis would require

more computer time, it would still be considerably shorter than that presently used in plane-wave simulations.

ACKNOWLEDGMENT

This work began while the author was at the Max-Planck-Institut für Plasmaphysik, Garching, and was completed at the University of California, Lawrence Livermore Laboratory. The author is indebted to Dr. H. Derfler for the hospitality extended by the Plasma Wave and Heating Group. Thanks are also due Dr. P. Mulser for many stimulating discussions. The author acknowledges useful conversations with Dr. K. Estabrook, Dr. J. Thomson, and Dr. W. Kruer, and thanks Prof. I. B. Bernstein for criticisms useful in the preparation of this paper. The work at Garching was done under terms of agreement on association with Euratom. The work at Livermore was performed with the support of U.S. DOE Contract No. W-7405-Eng-48.

APPENDIX: BOUNDARY CONDITIONS

Under the condition of Eq. (21)

$$k_0 r \ll \Delta X \ll |p^{-1}|\,, \tag{A1}$$

we integrate the right-hand side of Eq. (15) to find

$$a\delta E_x' + \int (a-1+n^2)E_x\,dX + 2\,\frac{\omega_c}{\omega}\,n\int a'\delta E_x\,dX - i\,\frac{\omega_c}{\omega}\int aE_y\,dX - in\int a'\delta E_y\,dX - i2\,\frac{\omega_c}{\omega}\,a\delta E_y' + inE_y = C_1 \tag{A2}$$

and

$$E_y' - a\delta E_y' - \int (a-1)E_y\,dX - 2\,\frac{\omega_c}{\omega}\,n\int a'\delta E_y\,dX - i\,\frac{\omega_c}{\omega}\int aE_x\,dX - in\int a'\delta E_x\,dX - 2i\,\frac{\omega_c}{\omega}\,a\delta E_x' - inE_x = C_2\,, \tag{A3}$$

where C_1 and C_2 are constants of integration. If we evaluate Eq. (A2) at X_2 and X_1 and subtract, we obtain

$$(a\delta E_x')_{X_1}^{X_2} + \int_{X_1}^{X_2}(a-1+n^2)E_x\,dX + 2\,\frac{\omega_c}{\omega}\,n\int_{X_1}^{X_2} a'\delta E_x\,dX - i\,\frac{\omega_c}{\omega}\int_{X_1}^{X_2} aE_y\,dX - in\int_{X_1}^{X_2} a'\delta E_y\,dX - i2\,\frac{\omega_c}{\omega}\,(a\delta E_y')_{X_1}^{X_2} + in(E_y)_{X_1}^{X_2} = 0\,. \tag{A4}$$

Assuming that the quantities a, E_x, and E_y are finite and smoothly varying across ΔX (whereas a' is a sharply peaked function), we can then approximate Eq. (A4) by

$$(a\delta E_x')_{X_1}^{X_2} + \langle a-1+n^2\rangle_x E_x\,\Delta X + 2\,\frac{\omega_c}{\omega}\,n\int_{X_1}^{X_2} a'\delta E_x\,dX - i\,\frac{\omega_c}{\omega}\,\langle aE_y\rangle_x\,\Delta X - in\int_{X_1}^{X_2} a'\delta E_y\,dX - i2\,\frac{\omega_c}{\omega}\,(a\delta E_y')_{X_1}^{X_2} + in(E_y)_{X_1}^{X_2} = 0\,, \tag{A5}$$

where the variables in angular brackets represent average quantities. Because $a\delta E_x' \approx E_x p^{-1} \gg E_x \Delta X$ and $a\delta E_y' \approx E_y p^{-1} \gg E_y \Delta X$, the second and fourth terms in (A5) are negligible when compared to the first and sixth terms, respectively. Thus, Eq. (A5) reduces to

$$\left[a\delta\left(E_x' - 2i\,\frac{\omega_c}{\omega}\,E_y'\right)\right]_{X_1}^{X_2} + inE_y\Big|_{X_1}^{X_2} + 2\,\frac{\omega_c}{\omega}\,n\int_{X_1}^{X_2} a'\delta\left(E_x - i\,\frac{\omega}{2\omega_c}\,E_y\right)dX = 0\,. \tag{A6}$$

Now if we integrate Eq. (A2) between X_1 and X_2 while assuming that E_y and $\int a'\delta[E_x - i(\omega/2\omega_c)E_y]\,dX$ are finite between X_1 and X_2, we find

$$\int_{X_1}^{X_2} a\delta\left(E_x' - 2i\,\frac{\omega_c}{\omega}\,E_y'\right)dX = 0\,. \tag{A7}$$

Similarly, we evaluate Eq. (A3) at X_2 and X_1 and subtract to obtain the expression

$$(E_y')_{X_1}^{X_2} - \int_{X_1}^{X_2}(a-1)E_y\,dX - 2\,\frac{\omega_c}{\omega}\,n\int_{X_1}^{X_2} a'\delta E_y\,dX - i\,\frac{\omega_c}{\omega}\int_{X_1}^{X_2} aE_x\,dX - \int_{X_1}^{X_2} a\delta E_y'\,dX - in\int_{X_1}^{X_2} a'\delta E_x\,dX - 2i\,\frac{\omega_c}{\omega}\,(a\delta E_x')_{X_1}^{X_2} - inE_x\Big|_{X_1}^{X_2} = 0\,. \tag{A8}$$

Because a, E_y, and E_x have been assumed finite and smoothly varying across ΔX, Eq. (A8) reduces to

$$(E_y' - inE_x)_{X_1}^{X_2} - \left[a\delta\left(E_y' + 2i\,\frac{\omega_c}{\omega}\,E_x'\right)\right]_{X_1}^{X_2} - in\int_{X_1}^{X_2} a'\delta\left(E_x - i2\,\frac{\omega_c}{\omega}\,E_y\right)dX = 0\,. \tag{A9}$$

By integrating Eq. (A3) between X_1 and X_2 while assuming that E_x and $\int a'\delta[E_x - i(2\omega_c/\omega)E_y]\,dX$ are finite, we obtain

$$(E_y)_{X_1}^{X_2} - 2i\,\frac{\omega_c}{\omega}\int_{X_1}^{X_2} a\delta\left(E_x' - i\,\frac{\omega}{2\omega_c}\,E_y'\right)dX = 0\,. \tag{A10}$$

Thus we have four equations, (A6), (A7), (A9), and (A10) that represent boundary conditions at a density discontinuity satisfying (A1). These conditions can be cast into more convenient forms in the following way. To obtain a first boundary condition, we multiply Eq. (A7) by $2i\omega_c/\omega$ and add to (A10), in which case we find, after integrating by parts,

$$\left\{E_y\left[1+\left(4\frac{\omega_c^2}{\omega}-1\right)a\delta\right]\right\}_{X_1}^{X_2} - 4\left(\frac{\omega_c^2}{\omega^2}-1\right)\int_{X_1}^{X_2} a'\delta E_y\,dX=0\,. \tag{A11}$$

To estimate the integral in Eq. (A11), we assume that at most E_y, which is finite, has a maximum value $E_{y\max}$. Then

$$\left|\int_{X_1}^{X_2} a'\delta E_y\,dX\right| \le |E_{y\max}|\int_{X_1}^{X_2} a'\delta\,dX = |E_{y\max}|\,(a\delta)_{X_1}^{X_2}\,. \tag{A12}$$

Using this argument in Eq. (A11) and neglecting terms of order $k_0^2r^2$, we find that (A11) gives the boundary condition

$$E_y\big|_{X_1}^{X_2}=0\,, \tag{A13}$$

i.e., E_y is continuous across the boundary.

Similarly, we can obtain a secondary condition by multiplying Eq. (A6) by $2i\omega_c/\omega$ and adding to Eq. (A9) while making use of (A13) to find

$$(E_y'-inE_x)_{X_1}^{X_2}=0\,, \tag{A14}$$

i.e., $\mathcal{H}_z$ is continuous across the boundary. Thus we have recovered the electromagnetic boundary conditions that are, of course, also valid for a plasma density with sharp boundaries.

A third condition at the boundary $X=0$ follows by making use of the electromagnetic boundary conditions in the previous analysis. Substituting Eq. (A13) back into (A6) or substituting (A14) back into (A9), integrating by parts, and neglecting terms of order $k_0^2r^2$ yields

$$\Gamma\equiv\{a\delta[E_x'-iE_y'+n(E_x-iE_y)]\}_{X_1}^{X_2}=0\,. \tag{A15}$$

Therefore, under the restriction given in Eq. (A1), we have three boundary conditions on the plasma slab, given by Eq. (A13)–(A15), i.e., continuity of E_y, $\mathcal{H}_z$, and Γ across $X=0$.

---

*Present address: Maxwell Laboratories, Inc., 9244 Balboa Ave., San Diego, Calif. 92123.

[1]M. Porkolab, Physica (The Hague) 82C, 86 (1976).

[2]J. Nuckolls, L. Wood, R. Thiessen, and G. Zimmerman, Nature (London) 239, 139 (1972).

[3]W. L. Kruer, Comments Plasma Phys. Controlled Fusion 2, 139 (1976).

[4]A. B. Langdon and B. F. Lasinski, Methods Comput. Phys. 16, 327 (1976).

[5]I. B. Bernstein and M. P. H. Weenink, Report No. 66/104, FOM-Institut voor Plasma-Fysica, Rijnhuizen, Jutphass, The Netherlands (1966) (unpublished); D. E. Baldwin, I. B. Bernstein, and M. P. H. Weenink, in *Advances in Plasma Physics*, edited by A. Simon and W. B. Thompson (Wiley, New York, 1969), Vol. 3, p. 85.

[6]G. A. Pearson, Phys. Fluids 9, 2454 (1966).

[7]D. E. Baldwin, J. Plasma Phys. 1, 289 (1967).

[8]J. C. deAlmeida Azevedo and M. L. Vianna, Phys. Rev. 177, 300 (1969).

[9]A. Sivasubramanian and T. Tang, Phys. Rev. A 6, 2257 (1972).

[10]L. D. Landau and E. Lifshitz, *Electrodynamics of Continuous Media* (Pergamon, Oxford, 1966), p. 242.

[11]P. Penfield, Jr., and H. A. Haus, *Electrodynamics of Moving Media* (MIT, Cambridge, Mass., 1967), p. 225.

[12]H. Hora, Phys. Fluids 12, 182 (1969).

[13]D. W. Forslund, J. M. Kindel, K. Lee, E. L. Lindman, and R. L. Morse, Phys. Rev. A 11, 679 (1975).

[14]A. L. Peratt and H. H. Kuehl, Radio Sci. 7, 309 (1972).

[15]V. L. Ginzburg, *The Propagation of Electromagnetic Waves in Plasma* (Pergamon, Oxford, 1970), Sec. 20.

[16]J. P. Freidberg, R. W. Mitchell, R. L. Morse, and L. I. Rudsincki, Phys. Rev. Lett. 28, 795 (1972).

[17]A. L. Peratt, Phys. Fluids 18, 1586 (1975).

[18]S. C. Brown, *Introduction to Electrical Discharges in Gases* (Wiley, New York, 1966), p. 167.

[19]M. N. Rosenbluth and R. Z. Sagdeev, Comments Plasma Phys. Controlled Fusion 1, 129 (1972); J. W. Shearer and J. J. Duderstadt, Nucl. Fusion 13, 401 (1973); W. L. Kruer and E. J. Valeo, Phys. Fluids 16, 675 (1973).

[20]R. B. White, C. S. Liu, and M. N. Rosenbluth, Phys. Rev. Lett. 31, 8 (1973).

[21]N. G. Denisov, Sov. Phys. JETP 4, 544 (1957).

[22]J. A. Stamper, K. Papadopoulous, R. N. Sudan, S. O. Dean, and E. A. McLean, Phys. Rev. Lett. 26, 1012 (1971).

[23]J. B. Chase, J. M. LeBlanc, and J. R. Wilson, Phys. Fluids 16, 1142 (1973).

[24]J. A. Stamper and D. A. Tidman, Phys. Fluids 16, 2024 (1973).

[25]J. J. Thomson, C. E. Max, and K. Estabrook, Phys. Rev. Lett. 35, 663 (1975).

[26]B. Bezzerides, D. F. DuBois, D. W. Forslund, and E. L. Lindman, Phys. Rev. Lett. 38, 495 (1977).

[27]W. F. DiVegilio, A. Y. Yong, H. C. Kim, and Y. C. Lee, Phys. Rev. Lett. 38, 541 (1977).

[28]B. Bezzerides, D. F. DuBois, and D. W. Forslund, Phys. Rev. A 16, 1678 (1977).

[29]C. E. Max, W. M. Manheiner, and J. J. Thomson, Phys. Fluids 21, 128 (1978).

[30]Wee Woo and J. S. DeGroot, Report No. PRG-23 Rev. 2, University of California at Davis, 1977 (unpublished).
[31]Wee Woo, K. Estabrook, and J. S. DeGroot, Report No. PRG-R-27, University of California at Davis, 1978 (unpublished).
[32]I. P. Shkarofsky, T. W. Johnson, and M. P. Bachynski, *The Particle Kinetics of Plasmas* (Addison-Wesley, Reading, Mass., 1966), p. 389.
[33]J. W. Shearer, Report No. UCID-15745, University of California, Lawrence Radiation Laboratory, 1970, p. 26 (unpublished).
[34]H. Hora, in *Laser Interaction and Related Plasma Phenomena*, edited by H. J. Schwarz and H. Hora (Plenum, New York, 1974), Vol. 3B; H. Hora, J. Opt. Soc. Am. 65, 882 (1975); H. Hora and E. L. Kane, Appl. Phys. 13, 165 (1977).
[35]Reference to a company or product name does not imply approval or recommendation of the product by the University of California or the U.S. Department of Energy to the exclusion of others that may be suitable.
[36]I. Fidone, G. Granata, and J. Teichmann, Phys. Fluids 14, 737 (1971).
[37]W. L. Kruer and K. G. Estabrook, Phys. Fluids 20, 1688 (1977).